Progress In Electromagnetics Research C, Vol. 101, 81–93, 2020

Optimization of a Rewritable Narrowband Filter in a SBN:75 Crystal

Luis A. Rubio-Saavedra[1, *], Birger Seifert[2], Pedro A. Márquez-Aguilar[3], and Adalberto Alejo-Molina[3, 4]

Abstract—We propose a rewritable optical frequency filter based on a volume Bragg grating recorded by holography on an SBN:75 photorefractive crystal. The theoretical results show the possibility of implementing a narrow-band filter whose reflectance is total for the characteristic wavelength of the third harmonic of the infrared for both TE and TM polarizations by optimizing the size of the interference fringes and the angle of incidence of the beam to be filtered, which must be close to 80 degrees.

1. INTRODUCTION

Stratified media, alternating periodic layers of material with different dielectric constants, have several applications in optics [1]. These periodic structures are classified according to the refractive index contrast, the size over which the periodicity is extended, the ratio of the spatial period to the wavelength of the light, etc.

The reflectivity achieved is determined by the number of layer pairs and by the refractive index contrast between the layer materials. The reflection bandwidth is determined mainly by the index contrast [2]. The required reflectivity and bandwidth are defined by the optical application. Mostly, high reflectivity is desirable. Bandwidth is not always as broad as possible. In notch filters, for example, very small bandwidth is required [3, 4].

Although Bragg reflectors are not a novel concept, different applications currently demand conventional Bragg gratings as in [5–8], to cite some. In the literature several works exist where bandwidth thickness is changed, and side-lobes are reduced by the use of complicated structures like nonuniform or modulated refractive index profiles [4, 9, 10]; however, this is difficult to achieve.

Holographic gratings recorded in photorefractive materials can be considered theoretically as dielectric Bragg gratings, because they alternate layers with different refractive indexes [11, 12]. Although holographic gratings have a sinusoidal profile of the index of refraction (rugate filters), we can assume it as a discrete multilayer stack, since they exhibit properties similar to a multilayer constructed from a series of discrete layers of alternate high and low indexes (index profile discrete), but without the higher-order reflection stopbands [13]. Thereby, the filter will retain only the beams at the fundamental reflection peak, namely, when light frequency is exactly the grating frequency (defined in Section 3), but not next reflection peaks corresponding to higher multiples. In certain applications where those other peaks are a problem, suppressing them will be quite satisfactory.

Holographic gratings have been recorded or fixed on photorefractive crystals such as $LiNbO_3$ or InP [14–16], which worked as optical filters. They could even be reconfigurable as in [15, 16]; however, the changes in the configuration depend on variables difficult to control such as temperature or external electric field, often possible only in the laboratory. More recently, more complex configurations of

Received 5 February 2020, Accepted 6 April 2020, Scheduled 17 April 2020

* Corresponding author: Luis Alberto Rubio-Saavedra (luis.rubio@uaem.mx).

[1] Facultad de Ciencias Químicas e Ingeniería, Universidad Autónoma del Estado de Morelos, Cuernavaca 62209, México. [2] Instituto de Física, Pontificia Universidad Católica de Chile, Santiago 7820436, Chile. [3] Centro de Investigación en Ingeniería y Ciencias Aplicadas, IICBA-UAEM, Cuernavaca 62209, México. [4] CONACYT — Centro de Investigación en Ingeniería y Ciencias Aplicadas, IICBA-UAEM, Cuernavaca 62209, México.

fixed grids in photorefractive materials have been proposed, such as waveguides designed for optical communications [17] in $LiNbO_3$ too, or superimposed several gratings recorded in photo-thermo-refractive materials designed for Ramman spectroscopy applications [18]. Liquid crystals are the most reconfigurable versions, and they are studied more [19].

On the other hand, highly efficient phase holograms can be recorded in SBN crystals, both in the external DC field [20, 21] and through the diffusion recording mechanism [22]. Undoped samples of SBN are transparent in the visible spectral region [23–25]. Furthermore, it allows multiple optical erasure of previously recorded holograms [26]. These characteristics make SBN a material suitable to assay a Bragg reflector based on holographic grating, which works like a frequency optical filter.

Unlike some Bragg reflectors made with other materials and techniques, in Bragg gratings of dielectric materials, obtaining high reflectivity as well as wide bandwidths is more complicated. The low contrast of the index of refraction presented by this type of gratings makes obtaining certain levels of performance rather a challenge. Features like layer thickness as thin as 266 nm [27] and refractive index modulation as small as 120×10^{-6} [28] are common in dielectric Bragg gratings recorded in photosensitive materials like photorefractive crystals. If the gratings are made of a few layers only, it is not easy to achieve 100% reflectance peaks, and the bandwidths will be rather narrow.

The optical frequencies that obey Bragg's law will be weakly reflected due to the small differences in the refractive indices between the layers of the holographic grid recorded in the SBN, so the total reflectance will be low. A simple idea has been studied by Yeh et al. [29] and Popov et al. [30] to improve bandwidth and reflectance in a dielectric Bragg grating with very low refractive index contrast. Fresnel theory says that the reflection intensity on an interface between two mediums increases with greater incidence angles. For example, incidence as grazing as 87.5° has been analysed and tested before on Bragg reflectors [31].

In this work, we put together different physical concepts to propose a filter. This filter is rewritable, in the sense that it can be tuned for blocking a wavelength. Our idea is that we take a photorefractive crystal as rewritable media, using holographic techniques, in particular the SBN:75 crystal. The assumption here is that after a period the charge distribution is stabilized, and it is possible to describe the material as a one-dimensional photonic crystal.

Then, this paper discusses, in the first section, our approach to photorefractivity, the distribution of charge, and how this changes the refraction index for making a grating. The second section is the photonic crystal description of the filter, using transfer matrix method. After that, in Section 3, the results are presented and discussed, where an additional formalism is used to compare the stop-gaps in the reflectivity, and this is coupled mode theory. Additionally, in this section, we present diffraction efficiency and phase diagrams. Finally, a summary and the conclusions are given.

2. PHOTOREFRACTIVE CRYSTAL DESCRIPTION

2.1. Photorefractivity and Photo-Induced Dynamic Gratings

The photorefractive effect is the change in refractive index of an optical material that results from the optically induced redistribution of electrons and holes. Under a wide range of conditions, the change in refractive index in steady state is independent of the intensity of the light that induces the change. Experiments are routinely performed using lasers of milliwatts of power. However, the effect tends to be rather slow, with the typical time of response of 0.1 seconds [32].

The origin of the photorefractive effect is illustrated schematically in Fig. 1. We imagine that a photorefractive crystal is illuminated by two intersecting beams of light of the same frequency. These beams interfere to produce the spatially modulated intensity distribution $I(x)$ shown in the upper graph. Free charge carriers, which we assume to be electrons, are generated through photoionization at a rate proportional to the local value of the optical intensity. These carriers can diffuse through the crystal or can drift in response to a static electric field [32].

In drawing the figure, we have assumed that diffusion is the dominant process, and in that case the electron density is minimum in the regions of maximum optical intensity, because electrons have preferentially diffused away from these regions. The spatially varying charge distribution $\rho(x)$ gives rise to a spatially varying electric field distribution or *space-charge field*, whose form is shown in the third

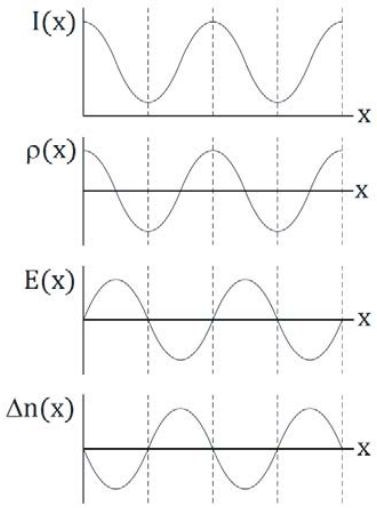

Figure 1. Origin of the photorefractive effect. (Adapted from Ref. [32]).

graph. The maxima of the field $E(x)$ are shifted by 90 degrees with respect to those of the charge density distribution $\rho(x)$.

The last graph in the figure shows the refractive index variation $\Delta n(x)$ that is produced through the linear electrooptic effect (Pockels effect) by the field $E(x)$. $\Delta n(x)$ is shifted by 90 degrees with respect to the intensity distribution $I(x)$ that produces it. This phase shift has the important consequence that it can lead to the transfer of energy between the two incident beams [32]. However, it is not important for this work where the maximum electric field magnitude will be employed to compute the maximum change of the index of refraction.

The width of the grating recorded in the photorefractive material (crystal SBN) is much larger than its spatial period. Therefore, a "thick" or "volume" hologram is generated. The diffraction within it plays a dominant role. In this case, the effect of diffraction of the light in the medium is called Bragg diffraction [33].

2.2. Space Charge Electric Field Estimation

The mechanisms of light-induced changes of optical materials properties are often described as having two steps. First, the light produces some material excitation, which then leads to a change of the optical properties. In the simplest case, the absorption and refraction of the material are changed depending on the stretch of the electric field, resulting in amplitude and phase gratings [34]. Absorption contribution is negligible, because the magnitude of the refractive index change (via the Pockels effect) is much greater than the absorption modulation. Therefore, formation of phase gratings or volume holographic gratings theory is briefly discussed below.

Stretch of the electric field $E(x)$ is required to compute the maximum $\Delta n(x)$ formed in the volume grating. Thus, it is possible to compute the electric field $E(x)$ analyzing the charge transport and associated equations for the case of an interference pattern of light, when it is projected onto the sample as schematically illustrated in Fig. 2.

The interference of two plane waves of complex amplitudes $\mathbf{S}(0)$ and $\mathbf{R}(0)$ that intersect at an angle 2θ produces a pattern of light (with spatial period Λ) onto the sample that is represented in Fig. 2.

The electric field depending on x is generated by the redistribution of photo-exited carriers, where diffusion is the only process of transport, is given by the expression

$$E(x) = mE_{\mathrm{D}} \frac{\sin Kx}{1 + m\cos Kx} \tag{1}$$

where the quantity m is called light fringes modulation or contrast; K is the spatial wave vector of the

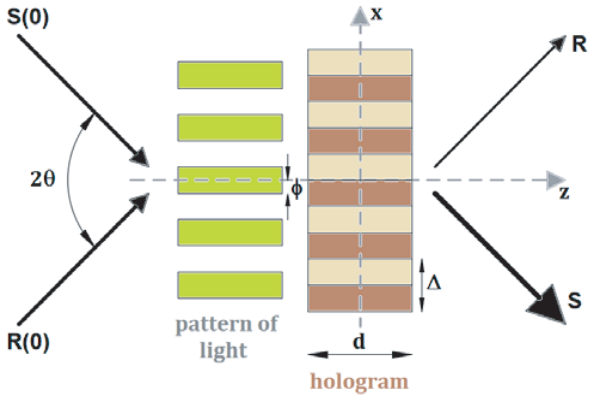

Figure 2. Recording of an interference volume hologram. The light pattern is displaced by ϕ with respect to the resulting pattern (Adapted from Ref. [35]).

grating $K \equiv 2\pi/\Lambda = 2k\sin\theta$; and E_{D} is the diffusion space-charge field

$$E_{\mathrm{D}} \equiv \frac{KD}{\mu} = K\frac{k_{\mathrm{B}}T}{e} \tag{2}$$

where μ and D are the mobility and diffusion constant for electrons ,respectively; e is the elemental charge; k_{B} is the Boltzmann constant; and T is the absolute temperature [35].

In accordance with Eq. (1), mE_{D} is the maximum value for $E(x)$. This parameter will be employed to compute maximum Δn in the holographic grating recorded in photorefractive material (SBN:75). Eq. (1) implies too that electric field profile is not sinusoidal. However, for the particular case which modulation is small ($|m| \ll 1$), behaviour is almost sinusoidal.

2.3. Modulation of the Refraction Index in Electro-Optic Crystals

Electric field $E(x)$ changes the dielectric permeability tensor ε_r of the material, and the modulation of the refraction index $\Delta n(x)$ appears (electro-optic effect) [34]. In some materials, the change in refractive index depends linearly on the strength of the applied electric field. This change is known as the linear electro-optic effect or Pockels effect [32].

The linear electro-optic effect can be described by a second-order nonlinear susceptibility. Therefore, the effect can occur only for materials that are non-centrosymmetric [32]. However, a very different formalism has historically been used to describe it. The complete development is extensive, and its study is not an objective of this work. The detailed development can be found in Refs. [32, 35, 36], to cite some sources.

To estimate the change of refraction index between the fringes of a holographic grating, it is enough to define that the Pockels effect for an anisotropic material is described by the change in the impermeability tensor [36]

$$\Delta\eta_{ij} = \eta_{ij}\,(E) - \eta_{ij}(0) = \sum_k r_{ijk}\mathbf{E}_k \tag{3}$$

which represents a nonlinear effect of second order. Here, $\eta_{ij}(E)$ is the impermeability tensor after the growth of the electric field; $\eta_{ij}(0)$ is the impermeability tensor before the illumination; r_{ijk} is a third rank tensor with $3^3 = 27$ elements called electro-optics coefficients; E_k represents the k component of space-charge field ($k = x, y, z$) and in general $\eta_{ij} = \varepsilon_0(\varepsilon)^{-1}_{ij}$ where ε_{ij} is the dielectric tensor and ε_0 the permittivity of vacuum [32].

Most photorefractive media are electro-optical anisotropic crystals. In these media, the dielectric tensor ε_{ij} is represented by a tensor of rank 2 and can be written in its main coordinate system as

$$\varepsilon_{ij} = \begin{pmatrix} \varepsilon_x & 0 & 0 \\ 0 & \varepsilon_y & 0 \\ 0 & 0 & \varepsilon_z \end{pmatrix} = \varepsilon_0 \begin{pmatrix} n_x^2 & 0 & 0 \\ 0 & n_y^2 & 0 \\ 0 & 0 & n_z^2 \end{pmatrix} \tag{4}$$

where ε_x, ε_y, and ε_z are the main dielectric constants, and n_x, n_y, and n_z represent the main refraction indexes [37]. According to these relations, Eq. (3) can be rewritten as

$$\Delta\eta_{ij} = \Delta\left(\frac{1}{n^2}\right)_{ij} = \sum_k r_{ijk}\mathbf{E}_k \tag{5}$$

The geometric representation of the tensor η_{ij} is a quadratic symmetric surface (ellipsoid) that is invariant to the coordinate system chosen [38]. After diagonalizing the tensor, it is possible to find the lengths that go from the centre to each end of the main axes of the ellipsoid. They are the magnitudes of the indexes of refraction n_x, n_y, and n_z.

Many crystals, such as SBN or $BaTiO_3$ for example, are uniaxial media, namely, $n_x = n_y = n_o$ (ordinary refractive index) and $n_z = n_e$ (extraordinary refractive index). This reduces the number of independent coefficients of the permeability tensor from 27 to 18, and the electro-optical coefficients are often written in terms of a 6×3 matrix, using a contracted notation. In fact, the number of independent coefficients decreases even more because many of them are zero.

According to the crystal symmetry of the SBN, which belongs to the 4 mm point group, the electro-optic tensor in the contracted notation is reduced to the form [32]

$$r_{ij} = \begin{bmatrix} 0 & 0 & r_{13} \\ 0 & 0 & r_{13} \\ 0 & 0 & r_{33} \\ 0 & r_{42} & 0 \\ r_{42} & 0 & 0 \\ 0 & 0 & 0 \end{bmatrix} \tag{6}$$

Substituting Eq. (6) in Eq. (5) leads to

$$\Delta\left(\frac{1}{n^2}\right)_{ij} = \begin{pmatrix} r_{13}E_z & 0 & r_{42}E_x \\ 0 & r_{13}E_z & r_{42}E_y \\ r_{42}E_x & r_{42}E_y & r_{33}E_z \end{pmatrix} \tag{7}$$

Depending on the direction in which the electric field is applied, its some components could be zero, and the modulation of the refractive index could affect either just n_o or n_e. A generalized expression of the amplitude of the refraction index modulation is

$$\Delta n = -\frac{1}{2}n^3 r_{\mathit{eff}} E_{\mathit{eff}} \tag{8}$$

where r_{eff} and E_{eff} are the effective values for these parameters [35]. The intensity of the electro-optical effect depends on the orientation of the space-charge field E within the crystal and polarization state of the light [37].

The quantity Δn obtained in Eq. (8) is the amplitude of the modulation of a grating such that if a beam of light travels through it, it passes through several holographic planes of the same refractive index several times. This volume grating is also called a Bragg grating.

3. FILTERS BASED ON BRAGG GRATINGS

Filters based on Bragg gratings use stratified structures with many interfaces which generate the required reflectance. A typical structure is depicted in Fig. 3. In this structure, one period is made of two alternating dielectric layers of refractive index n_1 and n_2, with thicknesses d_1 and d_2, respectively. Thus, one period is $\Lambda = d_1 + d_2$, which is also called a unit cell. Light beam travels along the axis of periodicity z with incident angle θ.

For a grating consisting of partially reflective planes, separated by a periodic distance, a round-trip phase is $2\varphi = 2k\Lambda\cos\theta$, where θ is the angle of incidence. Therefore, maximum reflection occurs when $2k\Lambda\cos\theta = 2q\pi$, i.e., when the Bragg condition is accomplished.

Considering the collaborative effects of all reflections then the obtained total reflectivity is considerably enhanced as illustrated in Fig. 4. This is the phenomenon whereby total reflection occurs not only at single frequencies that are multiples of $\nu_B/\cos\theta$, (where $\nu_B = c/2\Lambda$ is the Bragg frequency), but also over extended spectral bands surrounding these frequencies forming stopbands [38].

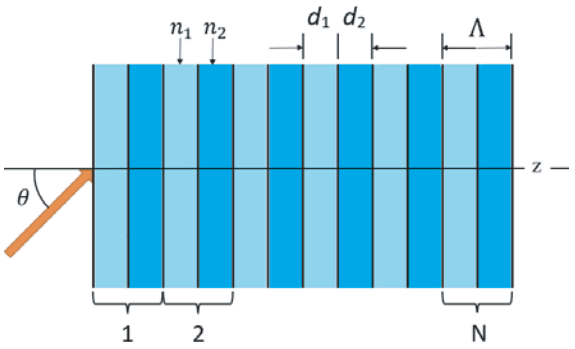

Figure 3. Bragg grating made with N identical segments.

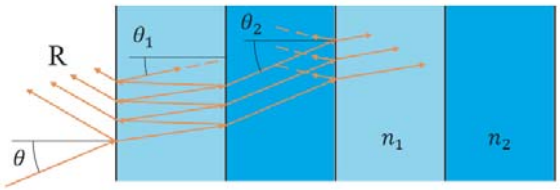

Figure 4. Collaborative reflections of an oblique optical wave on interfaces of stratified medium.

To develop an exact computation of the Bragg reflection, two arbitrary planes within a given optical system are considered, denoted by plane 1 and plane 2. The amplitudes of the forward and backward collected waves through plane 1 are represented by $E_1^{(+)}$ and $E_1^{(-)}$. Something similar happens with the plane 2. The process is illustrated in Fig. 5.

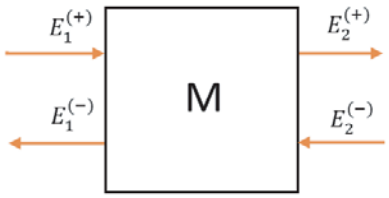

Figure 5. Forward and backward collected waves at plane 1 and plane 2, which depend on the medium properties represented by M.

In the figure, $E_1^{(+/-)}$ and $E_2^{(+/-)}$ are represented by a column matrix of dimension two. These two column matrices are related by the matrix equation

$$\begin{bmatrix} E_2^{(+)} \\ E_2^{(-)} \end{bmatrix} = \begin{bmatrix} A & B \\ C & D \end{bmatrix} \begin{bmatrix} E_1^{(+)} \\ E_1^{(-)} \end{bmatrix} \tag{9}$$

where matrix M, whose elements are A, B, C, and D, is called the wave-transfer matrix (transfer matrix method). It depends on the optical properties of the layered medium between the two planes.

Wave-transfer matrix is a fast and accurate analysis technique used for calculating the input and output fields for each identical segment. The output of the first matrix M_1 is used as the input to the second matrix M_2, not necessarily identical to M_1. The process is repeated until the entire complex profile grating is modelled. This method is capable of accurately simulating both strong and weak gratings, with or without chirp and apodization [39].

In our case, where each unit cell contains a periodic succession of two lossless dielectric layers, a reciprocal system satisfying the conservation relations for a lossless medium is formed, and it is represented by a generic unimodular wave-transfer matrix

$$\mathrm{M}_0 = \begin{bmatrix} 1/\mathrm{t}^* & \mathrm{r}/\mathrm{t} \\ \mathrm{r}^*/\mathrm{t}^* & 1/\mathrm{t} \end{bmatrix} = \begin{bmatrix} A & B \\ C & D \end{bmatrix} \tag{10}$$

where t and r are complex amplitude transmitivity and reflectivity, respectively, and $T = |\mathrm{t}|^2$ and $R = |\mathrm{r}|^2$ are the corresponding intensity transmittance and reflectance [38], respectively.

Considering a grating comprising a stack of N identical generic segments, each described by a wave-transfer matrix M_0, the wave-transfer matrix M for the N segments is simply the product $\mathrm{M} = \mathrm{M}_0^{\mathrm{N}}$.

The N^{th} power of the matrix M_0, with determinant $AD - BC = 1$, can be estimated by Sylvester's theorem [40]. In general, each of the $ABCD$ matrix elements in Sylvester's theorem may be complex. If in the relation $\sin\theta = (A + D)/2$ the right side of the equality is bigger than unity in magnitude (total-reflection regime, as will be seen later), θ is purely imaginary, and in that case, Sylvester's theorem may be written as [40]

$$M_0^N = \frac{1}{\sinh\Phi}\begin{bmatrix} A\sinh(N\Phi) - \sinh[(N-1)\Phi] & B\sinh(N\Phi) \\ C\sinh(N\Phi) & D\sinh(N\Phi) - \sinh[(N-1)\Phi] \end{bmatrix} \tag{11}$$

where $\Phi = \cosh^{-1}[(A + D)/2]$.

Substituting by the given values at Eq. (10), $\Phi = \cosh^{-1}[(A + D)/2]$ becomes

$$\Phi = \cosh^{-1}\left|\mathrm{Re}\left\{\frac{1}{t}\right\}\right| \tag{12}$$

Additionally, if we make

$$\Psi_N = \frac{\sinh[N\Phi]}{\sinh[\Phi]} \tag{13}$$

it is possible to rewrite Eq. (11) as

$$M_0^N = \Psi_N M_0 - \Psi_{N-1} I \tag{14}$$

Since the N-segment system is also lossless and reciprocal, its matrix may be written in the form

$$M_0^N = \begin{bmatrix} 1/t_N^* & r_N/t_N \\ r_N^*/t_N^* & 1/t_N \end{bmatrix} = \Psi_N M_0 - \Psi_{N-1} I \tag{15}$$

where t_N and r_N are the N-segment amplitude transmitivity and reflectivity, respectively.

Substituting and comparing the diagonal and off-diagonal elements of the matrices on both sides of the equation leads to

$$\frac{1}{t_N} = \Psi_N \frac{1}{t} - \Psi_{N-1} \tag{16}$$

$$\frac{r_N}{t_N} = \Psi_N \frac{r}{t} \tag{17}$$

Eqs. (16) and (17) define t_N and r_N in terms of t and r. Combining the two previous equations, the intensity transmittance $T_N = |t_N|^2$ is obtained. Using the relation $R_N = 1 - T_N$, it follows that the intensity reflectance of a multilayer reflector is given by

$$R_N = \frac{\Psi_N^2 R}{1 - R + \Psi_N^2 R} \tag{18}$$

where the factor Ψ_N is associated with the interference effects from collective reflections of the N segments, and R is the reflectance of a single segment [38].

This approach is used for both normal and oblique incident waves. The difference is that in the last case, Fresnel transmittances and reflectances at a boundary, t and r, are angle-dependent as well as polarization-dependent.

After transmission through a distance Λ (in this case a unit cell), the magnitudes of the forward and backward waves remain unchanged, and the phases are altered by a common shift Φ, called the Bloch phase. The interference factor Ψ_N depends on $\Phi = \arccosh|\mathrm{Re}\{1/t\}|$ for total reflection regime, i.e., regime where $|\mathrm{Re}\{1/t\}| = |\cos\Phi| > 1$, so that Φ is a complex variable, and the grating acts as a total reflector [38], when the material has no absorption.

The value of the argument $\mathrm{Re}\{1/t\}$ is derived from m_{11} element equal to $1/t^*$ of the matrix M_0 for light traveling at any angle trough a periodic system made for identical bilayers with refractive indexes n_1 and n_2, such that

$$\mathrm{Re}\left\{\frac{1}{t}\right\} = \frac{(\tilde{n}_1 + \tilde{n}_2)^2}{4\tilde{n}_1\tilde{n}_2}\cos(\tilde{\varphi}_1 + \tilde{\varphi}_2) - \frac{(\tilde{n}_1 - \tilde{n}_2)^2}{4\tilde{n}_1\tilde{n}_2}\cos(\tilde{\varphi}_1 - \tilde{\varphi}_2) \tag{19}$$

where $\tilde{\varphi}_1 = n_1 k_0 d_1 \cos\theta_1$ and $\tilde{\varphi}_2 = n_2 k_0 d_2 \cos\theta_2$ are the phases introduced by the two layers of a segment for waves with a generalized angle of incidence θ_1 in medium 1 and corresponding angle θ_2 in medium 2, so that $n_1 \sin\theta_1 = n_2 \sin\theta_2$; $\tilde{n}_1 = n_1 \cos\theta_1$ and $\tilde{n}_2 = n_2 \cos\theta_2$ are effective refractive indexes for TE polarization, and $\tilde{n}_1 = n_1 \sec\theta_1$ and $\tilde{n}_2 = n_2 \sec\theta_2$ for TM polarization [38].

In accordance with Fresnel theory, the larger the angle of incidence is, the larger the reflectance is. We are going to explore this to improve reflectance and bandwidth of a dielectric Bragg grating with very low index contrast, which shows a narrow band and low reflectance at normal incidence.

In order to plot the spectral total reflectance as a function of light frequency, taking into account the sum of the phases in Eq. (19) $\tilde{\varphi}_1 + \tilde{\varphi}_2 = n_1 k_0 d_1 \cos\theta_1 + n_2 k_0 d_2 \cos\theta_2$, we suppose that θ_1 is almost equal to θ_2 for very large angles of incidence and low difference between n_1 and n_2. In virtue of Snell law, the propagation angle θ_2 will be very little different from θ_1 when an optical wave passes into layer 2 from layer 1 in a unit cell. Hence, the sum $\tilde{\varphi}_1 + \tilde{\varphi}_2 = \pi\nu \cos\tilde{\theta} \Big/ \nu_B$ with $\tilde{\theta} = (\theta_1 + \theta_2)/2$, where $\nu_B = c/2\Lambda$ is the Bragg frequency.

4. RESULTS AND DISCUSSION

The theoretically proposed filter should work on a range of optical frequencies, whose spectral width depends greatly on the magnitude of the difference between the refractive indexes of the bilayers δn and the angle of incidence of the wave in the first layer θ_i. The greater the δn is, the wider width the stopband is according to Eqs. (12) to (19). The reflectance of a wave with a polarization state Transversal Electric (TE) or Transversal Magnetic (TM) is bigger if the angle of incidence is increased, according to the Fresnel theory.

As a result of projecting interference fringes with a spatial period $\Lambda = 390\,\text{nm}$ on an SBN:75 crystal ($n_o = 2.3117$, $n_e = 2.2987$ [36]) at normal orientation to the z-axis, a phase grating is generated. In areas with more intense lighting, there is a local change of the index of refraction generated via the linear electrooptic effect. This analysis shows changes whose values are $\Delta n_o \cong -0.00011348$ and $\Delta n_e \cong -0.00223337$, according to Eq. (8).

The electrooptic effect generates a modulation of the refractive indexes n_o and n_e as seen in Fig. 1. The amplitude of the modulation is the absolute value of Δn. Therefore, the maximum and minimum values of the ordinary and extraordinary indexes will be $n_o \pm |\Delta n_o|$ and $n_e \pm |\Delta n_e|$, respectively.

An optical perturbation with TE polarization, which propagates coplanar to the optical axis through the multilayer anisotropic optical medium, will undergo a phase change due only to the ordinary refractive index n_o, independent of the propagation angle θ_i. In contrast, a TM polarization wave will undergo a phase change due to gradually changing refractive index from n_e (if wave propagates completely perpendicular to z axis) to n_o (when the wave is collinear to the optical axis). In addition, as the propagation angle approaches zero degree, the only refractive index that governs the propagation is n_o, regardless of the polarization state of the light.

Thus, when the wave passing through the proposed filter is TE polarized, which will undergo changes due to the modulation of n_o, whose maxima and minima will be the refractive indexes of the periodic layers, designated as n_1 and n_2 in Figs. 3 and 4. According to the conditions of this work, the values resulting from these parameters are presented and summarized in Table 1.

In the case of the wave component with polarization TM, additional analysis is required. As mentioned above, the phase changes are due to the modulation of n_e, which depend on θ_i. Therefore, before estimating the values of n_1 and n_2, the propagation angle must be determined.

Table 1. Refractive indexes of the periodic layers corresponding to a specific propagation angle and polarization state of the light, resulting from the modulation of n via the electro-optical effect on the anisotropic material SBN:75 crystal. The last column shows the contrast of indexes between the layers.

Wave polarization	$\boldsymbol{\theta_i}$ [°]	$\boldsymbol{n_1}$	$\boldsymbol{n_2}$	$\boldsymbol{\delta n}$
TE	78.66	2.30989	2.31011	0.00022
TM	78.85	2.29697	2.30127	0.0043

To increase the width of the resulting stopband of reflectance, it is convenient that the propagation is an angle greater than zero degrees, due to the small value of the amplitude of the modulation $|\Delta n|$ of both indexes (which makes the δn very small). Then, the angle should cause that the reflectance at each interface increases and should be large enough to exceed the Brewster angle (where the reflectance drops to zero) in the case of TM polarization.

After optimizing the width d of the grating layers to maximize the δn between them, some incidence angles were tested for each polarization state (greater than the Brewster angle). Because the resulting frequency range within the stopbands corresponded to the near infrared, angles were adjusted such that the central wavelengths of the stopbands formed were approximately those corresponding to the third harmonic of the infrared (1064 nm). The resulting angles, as well as the refraction indexes of the periodic layers for the modulation of n_e, are also shown in Table 1.

Figures 6 to 8 show dependencies resulting from TE polarization analysis. Fig. 6 shows the theoretical results of the reflectance, according to Eq. (18). As mentioned above, the graph was generated assuming a spatial period of the holographic grating of 390 nm — that is, the thickness of each filter layer is 195 nm —, and the angle of incidence in the first layer of 78.66°. The figure corresponds to fundamental reflection peak (first stop-band), and the central wavelength is approximately 354.7 nm.

Results in Figs. 6, 8, 9, and 11 are expressed normalizing the light frequency to the spatial grating frequency, which is ν/ν_B. It makes possible match to any wavelength or grating period. For example, in Fig. 6, central wavelength of the stopband is 5.08, which means that light frequency would be five

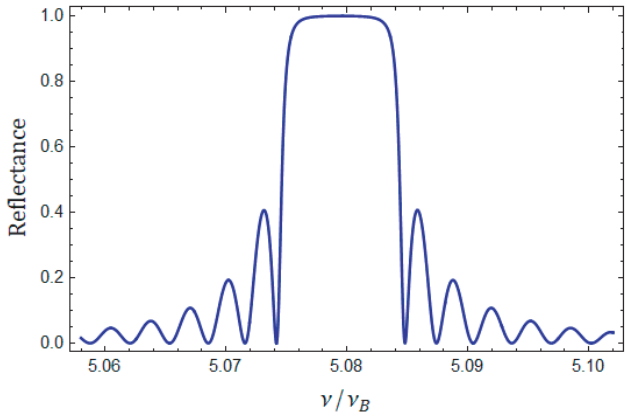

Figure 6. Spectral dependence of reflectance for TE polarization at incidence angle 78.66°.

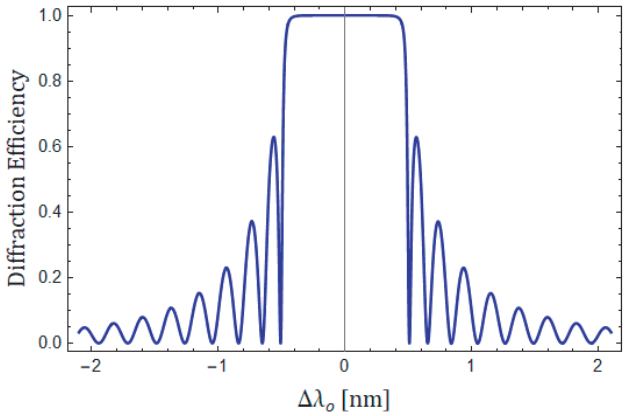

Figure 7. Dependence of diffraction efficiency on $\Delta\lambda_0$ for TE polarization.

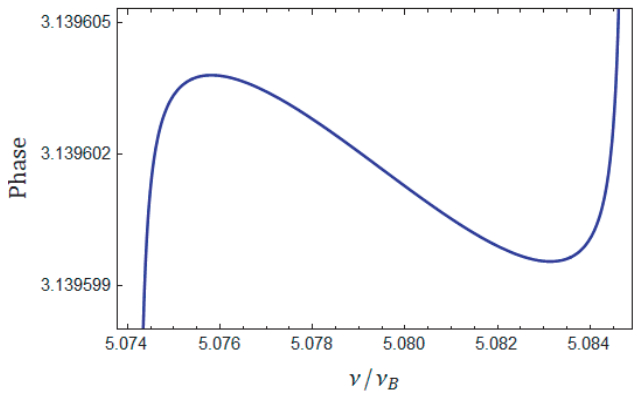

Figure 8. Estimated phase of the filter based on volume hologram for TE polarization.

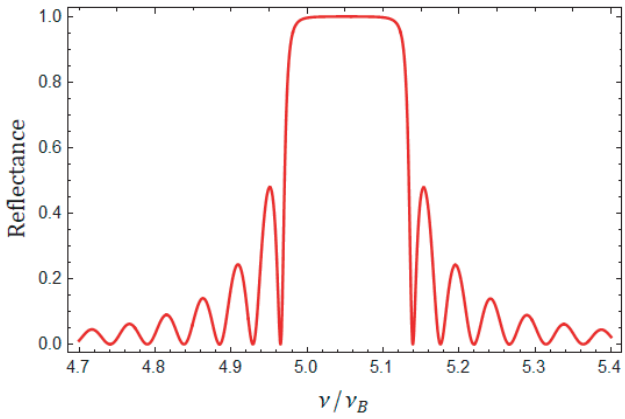

Figure 9. Spectral dependence of reflectance for TM polarization at incidence angle 78.85°.

point zero eight times of the Bragg frequency in order to achieve the performance of the grating.

In all the dependencies generated for TE polarization, the number of bilayers equal to 1500 was assumed, and an amount like that is easy to reach through holography, which is the proposal of this work.

An additional analysis to the formalism corresponding to the matrix theory of multilayer media is presented in Fig. 7. This result is obtained using coupled wave theory for a fixed grating, which is characteristic for holographic volume gratings.

The curve corresponds to the diffraction efficiency (rate between the intensity of the diffracted frequencies and the total intensity of a beam that propagates through a hologram) for an optical wave that propagates perpendicularly to the reflecting planes (reflection holograms [41]) and with an oblique angle of incidence, as a function of the change of the wavelength that satisfies the Bragg condition λ_0 (central wavelength of the stop-band), for the spatial period of the grating and the angle of incidence under study.

As observed, the spectral width of the formed stopband ($\approx$ 1 nm) corresponds to the estimate obtained from the curve of Fig. 6. In addition, frequencies of the stopband are also diffracted to one hundred percent, at least theoretically. These results support the previous results shown in the curve of Fig. 6.

Figure 8 shows an analysis of the phase just on the range of the first reflection stopband for TE polarization shown in Fig. 6. It is notorious that even when the curve decreases as the frequencies increase in the central part of the stopband, in fact, the values of the phase change millionths of π.

Figs. 9 to 11 show the dependencies resulting from the analysis with TM polarization. In particular, Fig. 9 shows the spectral dependence of the reflectance, according to Eq. (18). Once again, this graph was generated assuming a spatial period of the 390 nm of holographic grating. However, θ_i was adjusted to 78.85° so that the central wavelength retained the condition of being approximately the third harmonic of the infrared. As a result, the figure corresponds to the first stopband with $\lambda_0 = 354.9$ nm.

From Table 1, it is easy to identify that the difference of refractive indexes between layers δn, for the case of magnetic transversal polarization, is an order of magnitude larger than the case of the analysis with electric transversal polarization. This is due to the anisotropic nature of the photorefractive materials. Because of this fact, although Fresnel's theory says that a wave reflected in a TE polarization interface increases its reflectance more rapidly by increasing the angle of incidence than a wave with polarization TM, in our study, 100 bilayers are enough so that the reflectance stopband of a wave with TM polarization is well defined, as shown in Fig. 9.

The analysis of the diffraction efficiency shown in Fig. 10 corresponds to the reflection hologram with an oblique angle of incidence [41]. In this case, for TM polarization, the spatial period of the grating remains; however, the angle of incidence and the number of bilayers are adjusted to the values given in the previous paragraphs for this case.

According to the curve, the spectral width of the formed stopband ($\approx$ 20 nm) contrasts with

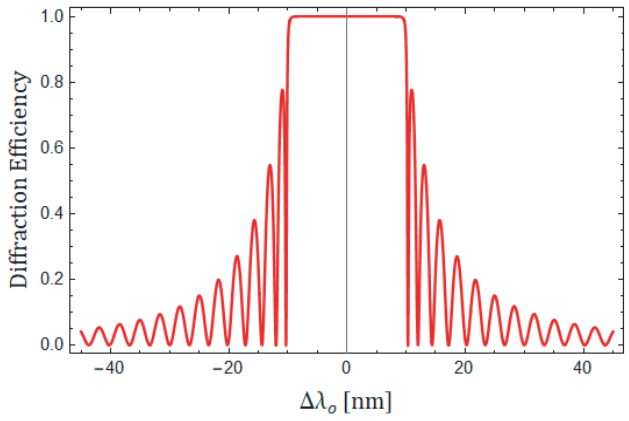

Figure 10. Dependence of diffraction efficiency on $\Delta\lambda_0$ for TM polarization.

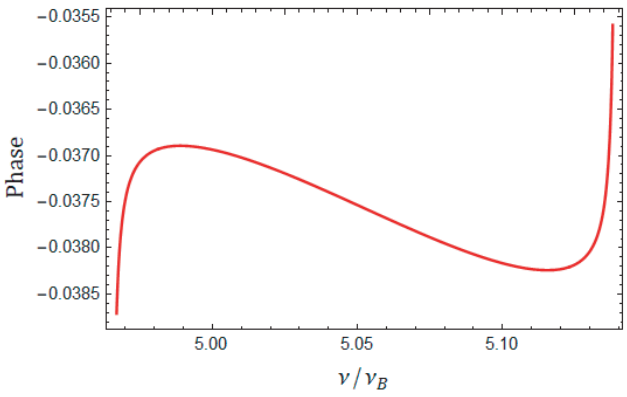

Figure 11. Estimated phase of filter based on volume hologram for TM polarization.

approximately 1 nm obtained in the TE polarization analysis. However, this amount also corresponds to the estimate obtained from Fig. 9, if the normalized frequencies are converted into wavelengths. Once again, these results support the dependence obtained through the matrix theory discussed previously.

Finally, Fig. 11 shows an analysis of the phase just in the range of the first stopband formed with the modulation of n_e for the angle of incidence of 78.85°. As in Fig. 8, it is remarkable as the phase remains almost constant. Since the phase function of the Bragg filter is almost constant, a laser pulse with the corresponding spectral bandwidth can pass through the Bragg filter without phase modulation. It means that the pulse is practically unmodified and therefore maintains its pulse duration almost perfectly.

In the best case, the contrast δn of the proposed grating is a few thousandths. If the propagation of the beam were normal to the reflecting planes, the reflectance achieved would be very low. Therefore, oblique propagation is decisive in the efficiency of Bragg reflection achieved in the previous graphs.

Another advantage of using grazing angles of incidence is that the total reflectance is achieved with indistinct TE and TM polarizations, as shown by Figs. 7 and 9. This ensures — at least theoretically — that the reflection of certain frequencies will be total, since the spectral range of reflection of the TE component is within the broadest spectral range of the TM component.

Spectral bandwidth is narrower in Figs. 6 and 7. However, notch filters or minus filters employ ranges very short too. Hence it is useful for some applications.

The grating proposed in this work supposes equal layer thicknesses. This makes it impossible to adjust thicknesses of alternating two layers to $\lambda/4$, namely, the wavelength region with higher reflectivity [8]. However, our theoretical results show that total reflectance is achievable.

5. CONCLUSIONS

We proposed and described a device that can be used as an optical filter by reflection, which can change the central wavelength by changing the angle of incidence of the beam and/or the thickness of the bilayers (spatial period of the holographic grating). The filter is based on volume holograms recorded on the SBN:75 photorefractive crystal. Theoretically, it could reach values close to 100% reflectance complying with the conditions described here.

In our dielectric grating, the refractive index contrast is small. However, it works perfectly as a Bragg grating. Our results show that the proposed filter achieves its best performance if a beam of light propagates with an angle of incidence between 78 and 79 degrees, which could be considered as grazing incidence. However, in [31] this type of incidence has been demonstrated.

If the angle of incidence decreases, the ability of the filter to fully reflect Bragg frequencies will still be possible by increasing the number of segments or bilayers of the reflector. However, holographic techniques in photosensitive materials make this feasible.

The performance of the filter was verified considering two different theories: "wave matrix theory" for multilayer media and "two beam coupling" for holographic gratings. A multilayer optical medium, with the physical characteristics presented in this work, should work experimentally as a filter of optical frequencies, for both TE and TM polarizations.

Therefore, we show theoretically that it is possible to build a rewritable filter by means of a Bragg grating recorded in a photorefractive crystal SBN, which can work in a range of propagation angles, filtering different wavelengths according to the Bragg law. However, the propagation angles must be large, almost grazing, with both TE and TM polarizations.

6. FUNDING STATEMENT

Consejo Nacional de Ciencia y Tecnología (CONACYT) [CB-2015-01/254617]. Millennium Institute for Research in Optics (MIRO).

ACKNOWLEDGMENT

L. A. R. S. gratefully acknowledged to "Consejo Nacional de Ciencia y Tecnología" (CONACyT-México) by the scholarship number 323855 provided. Also, L. A. R. S. thanks Ricardo Rojas Aedo from PUC,

Chile, for his help in this investigation.

A. A. M. thanks CONACyT for financial support during this research ("Theoretical Description of Nonlinear Optical Interactions for Surfaces and Bulk, Using Simplified Bond Hyperpolarizability Model and Group Theory").

Millennium Institute for Research in Optics (MIRO)

REFERENCES

1. Born, M. and E. Wolf, *Principles of Optics*, 7th edition, Cambridge University Press, Cambridge, 1999.
2. Paschotta, R, *Article on "Bragg Mirrors" in the Encyclopedia of Laser Physics and Technology*, 1st edition, Wiley-VCH, 2008, ISBN 978-3-527-40828-3.
3. Amotchkina, T. V., "Analytical estimations for the reference wavelength reflectance and width of high reflection zone of two-material periodic multilayers," *Applied Optics*, Vol. 52, No. 19, 4590–4595, 2013.
4. Hendrix, K. D., C. Hulse, G. J. Ockenfuss, and R. Sargent, "Demonstration of narrowband notch and multi-notch filters," *Proc. SPIE7067*, ID 706702, 2008.
5. Hehl, K., J. Bischoff, U. Mohaupt, et al., "High-efficiency dielectric reflection gratings: Design, fabrication, and analysis," *Applied Optics*, Vol. 38, No. 30, 6257–6271, 1999.
6. Berger, C., A. Lesnik, T. Zettler, et al., "Metalorganic chemical vapor phase epitaxy of narrow-band distributed Bragg reflectors realized by GaN:Ge modulation doping," *Journal of Crystal Growth*, Vol. 440, 6–12, 2016.
7. Guo, C., M. Kong, D. Lin, and B. Li, "Fluoride coatings for vacuum ultraviolet reflection filters," *Applied Optics*, Vol. 54, No. 35, 10498–10503, 2015.
8. Leem, J. W., X. Guan, and J. S. Yu, "Tunable distributed Bragg reflectors with wide-angle and broadband high-reflectivity using nanoporous/dense titanium dioxide film stacks for visible wavelength applications," *Optics Express*, Vol. 22, No. 15, 18519–18526, 2014.
9. Zhang, J., Y. Xie, X. Cheng, H. Jiao, and Z. Wang, "Thin-film thickness-modulated designs for optical minus filter," *Applied Optics*, Vol. 52, No. 23, 5788–5793, 2013.
10. Wang, X., H. Masumoto, Y. Someno, L. Chen, and T. Hirai, "Stepwise graded refractive-index profiles for design of a narrow-bandpass filter," *Applied Optics*, Vol. 40, No. 22, 3746–3752, 2001.
11. De Vré, R. and L. Hesselink, "Diffraction analysis of layered structures of photorefractive gratings," *Journal of Optical Society of America A*, Vol. 13, No. 2, 285–295, 1996.
12. Petrov, V. M., S. Lichtenberg, J. Petter, and T. Tschudi, "Control of the optical transfer function by phase-shift keying of a holographic Bragg grating," *Optics Communications*, Vol. 229, 131–139, 2004.
13. Macleod, H. A., *Thin-film Optical Filters*, 3rd edition, Institute of Physics Publishing, Bristol, 2001.
14. Müller, R., M. T. Santos, L. Arizmendi, and J. M. Cabrera, "A narrow-band interference filter with photorefractive $LiNbO_3$," *Journal of Physics D: Applied Physic*, Vol. 27, 241–246, 1994.
15. Müller, R., J. V. Álvarez-Bravo, L. Arizmendi, and J. M. Cabrera, "Tuning of photorefractive interference filters in $LiNbO_3$," *Journal of Physics D: Applied Physic*, Vol. 27, 1628–1632, 1994.
16. Hervé, D., M. Chauvet, J. E. Viallet, and M. J. Chawki, "First tunable narrowband 1.55 µm optical drop filter using a dynamic photorefractive grating in iron doped indium phosphide," *Electronics Letters*, Vol. 30, No. 22, 1883–1884, 1994.
17. Hukriede, J., D. Runde, and D. Kip, "Fabrication and application of holographic Bragg gratings in lithium niobate channel waveguides," *Journal of Physics D: Applied Physics*, Vol. 36, R1–R16, 2003.
18. Glebov, A. L., O. Mokhuna, A. Rapaport, S. Vergnole, V. Smirnov, and L. B. Glebov, "Volume Bragg gratings as ultra-narrow and multiband optical filters," *Proc. of SPIE*, Vol. 8428, ID 84280C, 2012.

19. Sutherland, R. L., V. P. Tondiglia, L. V. Natarajan, et al., "Liquid crystal Bragg gratings: Dynamic optical elements for spatial light modulators," *Proc. of SPIE*, Vol. 6487, ID 64870V, 2007.
20. Thaxter, J. B., "Electrical control of holographic storage in Strontium-Barium Niobate," *Applied Physics Letters*, Vol. 15, No. 7, 210–212, 1969.
21. Thaxter, J. B. and M. Kestigian, "Unique properties of SBN and their use in a layered optical memory," *Applied Optics*, Vol. 13, No. 4, 913–924, 1974.
22. Voronov, V. V., É. K. Gulanyan, I. R. Dorosh, et al., "Photoelectric and photorefractive properties of cerium-doped barium strontium niobate crystals," *Soviet Journal of Quantum Electronics*, Vol. 9, No. 9, 1172–1175, 1979.
23. Ballman, A. A. and H. Brown, "The growth and properties of strontium barium metaniobate, $Sr_{1-x}Ba_xNb_2O_6$, a tungsten bronze ferroelectric," *Journal of Crystal Growth*, Vol. 1, No. 5, 311–314, 1967.
24. Neurgaonkar, R. R., W. K. Cory, J. R. Oliver, M. D. Ewbank, and W. F. Hall, "Development and modification of photorefractive properties in the tungsten bronze family crystals," *Optical Engineering*, Vol. 26, No. 5, 392–405, 1987.
25. Dorosh, I. R., Y. S. Kuzminov, N. M. Polozkov, et al., "Barium-strontium niobate crystals for optical information recording," *Physica Status Solidi (A)*, Vol. 65, No. 2, 513–522, 1981.
26. Thaxter, J. B. and M. Kestigian, "Unique properties of SBN and their use in a layered optical memory," *Applied Optics*, Vol. 13, No. 4, 913–924, 1974.
27. Golmohammadi, S. and A. Rostami, "Optical filters using optical multi-layer structures for optical communication systems," *Fiber Integrated Optics*, Vol. 29, No. 3, 209–224, 2010.
28. Smirnov, V., J. Lumeau, S. Mokhov, B. Y. Zeldovich, and L. B. Glebov, "Ultranarrow bandwidth moiré reflecting Bragg gratings recorded in photo-thermo-refractive glass," *Optics Letters*, Vol. 35, No. 4, 592–594, 2010.
29. Yeh, P., A. Yariv, and C.-S. Hong, "Electromagnetic propagation in periodic stratified media. I. General theory," *J. Opt. Soc. Am.*, Vol. 67, No. 4, 423–438, 1977.
30. Popov, K. V., J. A. Dobrowolski, A. V. Tikhonravov, and B. T. Sullivan, "Broadband high-reflection multilayer coatings at oblique angles of incidence," *Applied Optics*, Vol. 36, No. 10, 2139–2151, 1997.
31. Eriksson, F., G. A. Johansson, H. M. Hertz, E. M. Gullikson, U. Kreissig, and J. Birch, "14.5% near-normal incidence reflectance of Cr/Sc x-ray multilayer mirrors for the water window," *Optics Letters*, Vol. 28, No. 24, 2494–2496, 2003.
32. Boyd, R. W., *Nonlinear Optics*, 2nd edition, Academic Press, San Diego, 2003.
33. Petrov, M. P., S. I. Stepanov, and A. V. Khomenko, *Photorefractive Crystals in Coherent Optical Systems*, Springer-Verlag, Berlin, 1991.
34. Eichler, H. J. and A. Hermerschmidt, "Light-induced dynamic gratings and photorefraction," *Photorefractive Materials and Their Applications 1, Basic Effects*, P. Günter and J.-P. Huignard, Eds., 7–28, Springer, New York, 2006.
35. Frejlich, J., *Photorefractive Materials, Fundamental Concepts, Holographic Recording and Materials Characterization*, Wiley-Interscience, Hoboken, 2007.
36. Yariv, A. and P. Yeh, *Photonics: Optical Electronics in Modern Communications*, Oxford University Press, New York, 2007.
37. Denz, C., M. Schwab, and C. Weilnau, *Transverse-Pattern Formation in Photorefractive Optics*, Springer-Verlag, Berlin, 2003.
38. Saleh, B. E. A. and M. C. Teich, *Fundamental of Photonics*, 2nd edition, Wiley-Interscience, Hoboken, 2007.
39. Kashyap, R., *Fiber Bragg Gratings*, 2nd edition, Academic Press, San Diego, 2010.
40. Tovar, A. A. and L. W. Casperson, "Generalized Sylvester theorems for periodic applications in matrix optics," *J. Opt. Soc. Am. A*, Vol. 12, No. 3, 578–590, 1995.
41. Kogelnik, H., "Coupled wave theory for thick Hologram Gratings," *The Bell System Technical Journal*, Vol. 48, No. 9, 2909–2947, 1969.